remote sensing

MDPI

Article

Insect Monitoring Radar: Maximizing Performance and Utility

V. Alistair Drake [1,2,*], Shane Hatty [1,3], Colin Symons [1,4] and Haikou Wang [5]

1 School of Science, UNSW Canberra, The University of New South Wales, Canberra, ACT 2610, Australia; shane.hatty@gmail.com (S.H.); C.Symons@westernsydney.edu.au (C.S.)
2 Institute for Applied Ecology, University of Canberra, Canberra, ACT 2617, Australia
3 Now at PO Box 154, Lobethal, SA 5241, Australia
4 Now with Western Sydney University Penrith, Penrith, NSW 2751, Australia
5 Australian Plague Locust Commission, Canberra, ACT 2601, Australia; Haikou.Wang@agriculture.gov.au
* Correspondence: a.drake@adfa.edu.au

Received: 11 January 2020; Accepted: 5 February 2020; Published: 11 February 2020

Abstract: Autonomously-operating radars employing the 'ZLC configuration' have been providing long-term datasets of insect flight activity to heights of about 1 km since the late 1990s. A unit of this type operating in Australia has recently received a major upgrade. The aim of the project was to maximize the utility of the radar to entomologists and aeroecologists by providing larger and more continuous datasets and extending observations to 2.5 km. The upgrade was achieved primarily by incorporating modern digital technology, which provides much improved data-acquisition-and-control performance and data-archiving capacity; by implementing a more comprehensive observing protocol; and by replacing fixed electronic signal-acquisition gates with specially developed software that identifies insect echoes and applies a narrow moving gate that follows them. The upgraded version provides an approximately five-fold increase in hourly sample sizes, a doubling of the duration of observations (from 12 to 24 h per day) and a doubling of the height range over which observations are made. The design considerations (incentives and constraints) that informed the various subsystem implementations are identified, and the necessary compromises are discussed. Observations of the development of a layer echo during a migration by two different insect types are presented as a demonstration of the upgraded unit's capabilities.

Keywords: radar; insect; migration; aeroecology; signal gating; ZLC configuration

1. Introduction

Radars that are specifically designed for long-term observations of insects flying at heights up to around 1 km were first deployed around 1990 [1]. From the late 1990s, a design employing the 'ZLC (Zenith-pointing Linear-polarized Conical scan) configuration' [2], in which the beam incorporates both rotating linear polarization and a very narrow angle conical scan (sometimes termed 'nutation'), has predominated. Known variously as IMRs ('insect monitoring radars' [2]) or VLRs ('vertical-looking radars' [3]), units of this type have been operated over extended (multiple-year) periods in Australia, China, Japan, and the UK. Long-term data from these radars have led to advances in the understanding of migratory behaviour and its ecological consequences (e.g., [4,5]) and have also provided support for operational pest forecasting [6]. Observations from small, purpose-built radars such as these complement the data on insect movement that are now becoming available from operational weather-surveillance radars (WSRs, e.g., [7]). The narrow beam, high range resolution, and short observing range of the IMRs and VLRs allow them to resolve individual insects, enabling the discrimination of different target types [8,9] and the examination of within-population variances

of migration parameters (e.g., [10]). The relatively low capital and running costs of these units make them more compatible with the modest budgets typical of entomological and aeroecological research programs.

The original IMR and VLR implementations were developed during the 1990s and incorporated technologies that were available and affordable at that time. As subunits have aged and come to need repair or replacement, more modern equipment has been introduced, either through necessity—as superseded components became unavailable—or to take advantage of improved performance and reliability. In the case of the IMRs operating in Australia, opportunities provided by new data-acquisition technologies have led to a more general review of the systems' design and operating protocols, as well as recognition that an IMR's effectiveness as a facility for observing insect migration could be considerably increased. Experience gained through analysing IMR data from over a decade (e.g., [6,10,11]) also informed this review by indicating circumstances where larger datasets, or more continuous observation, would likely have enabled additional or stronger scientific inferences. An upgraded unit, designated IMRU ('IMR Upgraded'), was subsequently developed and deployed to Hay, New South Wales, Australia (34.5458°S, 144.8663°E), where it commenced observations in August 2017.

In this paper, the main features of the IMRU that distinguish it from its predecessors are outlined, the methods used to enhance its performance are described, and example observations that illustrate its capabilities are presented. The essential features of the ZLC configuration—vertical beam, rotating polarization, and narrow-angle scan—are unchanged, as is the antenna assembly that implements this [12] (ch. 5). In its external appearance, therefore, the unit resembles an IMR (Figure 1). The IMRU also continues to rely on an X-band transceiver that is derived from a commercial civil-marine radar (BridgeMaster E, Northrop Grumman Sperry Marine, New Malden, UK); this employs pulse transmission (25 kW peak power) and operates non-coherently. The innovations presented here relate to the radar's operating protocols and the initial processing, both in hardware and software, of the echo signals. The extracted echo signals differ little from those from an IMR, and the algorithm for retrieving trajectory and target-character parameters from these signals [12] (ch. 7) [13] did not require modification. The upgraded version provides an approximately five-fold increase in hourly sample sizes, a doubling of the duration of observations (from 12 to 24 h per day), and a doubling of the height range over which observations are made.

Figure 1. IMRU equipment cabin and antenna, Hay, New South Wales (NSW), April 2017.

The IMRU may represent the limits of what non-coherent radar technology—now superseded in many other applications—can deliver for entomological observation. However, much of what

is described here would be transferable to a ZLC unit that employs FMCW or pulse-compression techniques (see, e.g., [12] (ch. 8)) or even to a fully-polarimetric vertical-beam design [14]. The paper discusses the design considerations behind each upgrade element, and this should assist the application of these methods in other contexts.

2. Materials and Methods

A full specification of the IMRU is provided in Table 1.

Table 1. Key IMRU design features and parameters.

Subsystem, Operation.	Parameters, Features.
Frequency/wavelength	9.4 GHz/3.2 cm (X-band).
Transmitter	Pulsed, 25 kW peak power (nominal), repetition frequency 960 Hz, pulse duration 0.05 μs ('S-mode'), 0.25 μs ('M-mode').
Receiver	Non-coherent, logarithmic amplification; bandwidth ~20 MHz, minimum detectable signal −90 dBm.
Antenna	Parabolic reflector, diameter 1.8 m, directed vertically; gain 43 dB; losses (radome, waveguide) ~3 dB (two way).
Beam	Circular pencil beam (full width at half maximum 1.1°), Gaussian intensity pattern.
Scan	Narrow-angle conical, offset 0.24 beam-widths. 450 r.p.m. (7.5 Hz, period 0.133 s, alternating clockwise and anticlockwise at hourly intervals).
Polarization	Linear, turning synchronously with conical scan [a]; E-field aligned with offset direction.
Sampling (fast time)	Video transformed into −5 to +5-V range and sampled at 60 or 120 MHz [b] over 0–9 μs (S-mode, 0–1350 m in range) or 8–17 μs (M-mode, 1200–2550 m); 540 or 1080 samples per pulse.
Sampling (slow time)	960 Hz (128 fast-time sequences per scan cycle).
Observing protocol	15-min cycle comprising 3 S-mode and 1 M-mode observing periods, each of 3-min duration.
Operation	Continuous ("24/7"), fully automatic, with self-testing (multiple features) and autonomous recovery.

[a] As polarization is axial, the modulation produced is double the scan rate, i.e., 15 Hz. [b] The 120-MHz rate provides greater precision and is preferred. The 60-MHz rate functions satisfactorily and allows for fast sampling on a second channel for system-integration testing.

2.1. System and Protocol Upgrades

2.1.1. "24/7" Observing and Data Storage

Radars produce very large quantities of information, and in the 1990s, data-storage (and more particularly, archiving) limitations provided a constraint on the number of observations that it was practicable to record—at least when ZLC technology was still new and it seemed appropriate to retain the 'raw' (i.e., as-acquired) data. Accordingly, IMRs operated only during night-time hours—as the species of primary interest, the Australian plague locust *Chortoicetes terminifera* and a variety of noctuid moths, were known to be nocturnal migrants—and recorded for only about 30 min in every hour. VLRs, which immediately process the acquired data and record only small samples of the original signals, operate throughout the day and night [3]. This latter approach was adopted for the IMRU, which runs on a 15-min cycle: 12 min are allocated to observation, and the remainder are allocated to an initial processing stage ('preprocessing'), writing the preprocessed data to disk, recording temperature and rain, backing the data up, and self-testing. Two cycles a day are sacrificed for (i) full processing of the day's acquired data and (ii) a full system reboot; these are scheduled for, respectively, early morning and mid-afternoon—when experience suggests that transient phenomena of entomological or aeroecological interest are less likely to occur. Voucher files of 30 s of unprocessed signal data are also recorded four times a day to allow for a retrospective analysis of the radar's performance; these files have also been used to develop and refine the preprocessing algorithm. With terabyte data drives now readily affordable and preprocessing essential (see below), data storage is no longer a constraint on operations.

2.1.2. Observing to 2.5 km

IMRs, VLRs, and other ZLC implementations have so far employed pulse transmission with 'short' pulses (0.05 or 0.07 μs duration and 7.5 or 10.5 m effective length), and recorded echoes out to heights of around 1.3 km ('S-mode' [3,6]). While larger insects such as *C. terminifera* (mass ~400 mg for a migration-capable adult [9]) are detectable well above this, the successful analysis of the echo signals, leading to retrieval of all trajectory and target-character parameters, requires a strong echo that remains clear of the radar receiver's electronic noise for several antenna-rotation cycles. For an IMR, the limiting

height has been empirically shown to be around 800 m for 'small' insects (~30 mg), 1000 m for 'medium' ones (~50 mg), and (by extrapolation) around 1700 km for 'large' ones (~250 mg) [15]. To enable the observation of migration at greater heights, the IMRU switches to 'medium'-pulse (0.25 μs, 37.5 m) transmission for 3 min of each 15-min observing cycle. While in this 'M-mode,' data are acquired at ranges of 1200–2550 m. There is a 150-m deep overlap region with the S-mode observing range of 0–1350 m to allow for a comparison of performance of the two modes. A short pulse is preferable at lower heights because it reduces the likelihood of interference between the echoes from nearby targets; this is less of a problem above 1200 m, as insect densities are usually lower there. The divergence of the radar beam means that insect transit times, and therefore signal sequences, are longer in M-mode observations (because of the target's greater height), and it seems plausible that this compensates for slower and less strong modulations due to the broader beam. The M-mode echoes have been found to satisfactorily process with the retrieval algorithm developed for the IMRs [13], so no modifications were needed.

2.1.3. Scan Speed and Direction

To retrieve speed and direction, echo signals that extend over several rotation cycles of the narrow-angle scan are required. As the beam is quite narrow at low altitudes (8–10 m at 300 m [15]) and insect speeds of ~10 m s^{-1} are commonplace at these heights, a scan rate of at least a few cycles per second is therefore needed. (A broader beam, produced by a lower-gain antenna, is not a viable alternative because at longer ranges, the horizontal resolution would be poor—leading to more frequent interference from nearby targets—and the echo signals would be weak.) The IMR used a scan rate of 5 Hz (300 rev/min). The scan also produced, via an angle encoder, a pulse train that was used to trigger the radar's transmitter; with 256 pulses per cycle, a pulse repetition frequency (PRF) of 1280 Hz, which is just below the transmitter's nominal maximum of 1300 Hz, was obtained. For the IMRU, the scan rate was increased to 7.5 Hz (450 rev/min), and the encoder output was reduced to 128 per cycle for a PRF of 960 Hz. The reduced average power output due to the lower PRF corresponds to a performance loss, assuming effective pulse-to-pulse averaging, of ~1 dB, but this is compensated for by 50% more cycles being available to the retrieval algorithm for estimating modulations. An increase in the scan rate to 10 Hz would eliminate the loss, but this has not been implemented because of concerns about the mechanical stability and integrity of the offset antenna feed—which already incorporates a counterweight to minimize centrifugal stress [12] (ch. 5).

A question of current interest in insect migration studies that has been addressed mainly through ZLC-radar datasets, is the relationship between the insect's orientation (or heading) and its direction of movement (or track). For some insect classes, biases to the left or the right have been observed [16]. As IMRs and VLRs operate with clockwise and anticlockwise rotation, respectively, concerns that such biases might be an artefact of the rotation direction could arise. A consideration of data-acquisition and parameter-retrieval processes do not support this, but doubts can be further reduced by simply reversing the rotation direction from time to time. The IMRU does this every hour, scanning clockwise on even hours and anticlockwise on odd. Modification of the retrieval algorithm has been minimized by treating all observations as clockwise until the end when, if rotation was in fact anticlockwise, the angle variables are transformed appropriately before being written to the output file.

2.1.4. Elimination of Stationary-Beam Observations

The IMRs spent ~8 min in each hour observing with no scan rotation [17], as this was initially thought to be necessary to retrieve wingbeat frequencies (which have value for target identification). These observations had little general utility, as, without the scan, few other parameters could be retrieved. It was later determined that wingbeats could often be detected even in the highly variable scanning-beam signals [18], and these have proven much more valuable because they can be associated with other target-character parameters that are retrieved from the same echo. This leads to more confident assignments of individual echoes to different target classes—and, indeed, to more

sophisticated methods for recognizing those classes [8,9]. Accordingly, stationary beam observations have been eliminated from the IMRU's operating protocol, and the time occupied by them has been reallocated to scanning-beam observations to improve the continuity and sample size of these.

Stationary-beam observations require the radar's PRF to be generated in an alternative way, and this facility was retained in the IMRU implementation so that this observation type could be reinstated; a practical option might be to assign the last 15-min cycle in each hour to stationary-beam operation. Wingbeat-frequency distributions that are produced with a stationary beam would be of better quality than those currently available, in which artefactual peaks at low harmonics of the scan-rotation rate (e.g., 15, 22.5, and 30 Hz) are often present.

2.1.5. Self-Test and Auto-Recovery

To support their autonomous operation, IMRs incorporated a range of self-test features to monitor their performance and terminate operation in the event of a fault developing, as well as a mechanism for recovery from failures when these occured [19]. Remote access via a telephone link and modem enabled daily downloads of data summaries, and fault-finding and even reprogramming were possible without the need for a site visit. These facilities have largely been carried over to the IMRU, where they have been implemented with more modern technology and, in some instances, strengthened. Communication is now done via mobile telephony (using the 3G technology currently available at the radar site; Unimax MA-2025, Maxon Australia, Seven Hills, Australia) and a remote desktop connection (RDC; Microsoft Ltd., Redmond, WA, USA), which allows for full access to the radar's control computer. All subunits, apart from the signal-acquisition system, are monitored and controlled via a USB connection to a multifunction card (USB6259, National Instruments, Austin, TX, USA). Self-testing extends to temperature (at 3 points—one inside the cabin, one outside in the cabin's shade, and one on the motor under the antenna—with the termination of operation if any of these record a temperature exceeding 45 °C); mains power—supplied via an uninterruptible power supply (Powerware 9125, Eaton Corporation, Raleigh, NC, USA) to allow for a controlled termination in the event of a power cut; scan rotation rate; current drawn by the scan motor; scan internal alignment (to detect possible drive-belt slippage); PRF; and outputs from the transceiver's BITE ('built-in test equipment') that include a tune indicator and the magnetron current. Transceiver performance is also monitored by means of a resonant cavity (65125V, Decca Marine Radar, London, UK) that is fed from the waveguide connecting the transceiver to the antenna. During tests, the tune voltage is varied, the value at which echo intensity is greatest is determined, and this value and the maximum intensity are recorded. When not in use, the cavity is switched out of tune with a solenoid so that no unwanted echo is produced. The transceiver's auto-tune facility is activated for actual observations as it has proven reliable.

Self-testing is undertaken during the 3 min in each 15-min cycle that is not used for observations and follows a schedule that ensures that each test occurs at least once every hour. Test outputs are recorded to a log file, along with details of the acquired signal data (times, file names, duration of data-acquisition period and of preprocessing, number of identified echoes, etc.), temperatures, and output from a rain detector. An inspection of the log file via RDC provides a means of determining whether the unit is functioning well and of diagnosing any faults. Operations are not terminated during rain, but the logged rain indications could be helpful when interpreting the observations. Other weather factors can be obtained from automatic weather stations (AWSs) operated at locations close to the radars by the Australian Bureau of Meteorology, so a dedicated AWS that is linked to the radar, as initially implemented with the IMRs [19], is no longer required. The scheduling system also manages the backing up of each day's data to a removeable terabyte drive.

If self-testing indicates a fault, the radar is closed down in a controlled way. A timer program then runs until 10 min before the following hour, when the main program is restarted. (The two programs are chained via a simple control file.) In some cases, normal operation resumes on the hour, and no more than 1 h of observations are lost. If the fault is persistent, this cycle continues until noticed via the

RDC link, when the main program can be disabled and the radar left dormant until the next servicing visit. Some self-test quantities vary considerably (e.g., motor current, according to temperature), and appropriate thresholds for termination have not yet been fully established. Self-test faults sometimes arise in the self-testing sensors or circuitry itself, and when this can be determined to be the case, it is usually straightforward to implement a 'work-round'—i.e., to bypass the test with a minor software modification that can be undertaken remotely via RDC—and to quickly return the radar to operation.

The IMRU undergoes an auto-recovery procedure each day at 16 h to bring it back into operation in the event of a fault that causes the control computer or the communication link to cease responding to commands. If the unit is operating normally, the scheduling software terminates observations, and the computer idles. An independent timer unit then cycles the power, causing the computer to reboot and commence its normal start-up protocol. A second timer cycles the power to the motor's proprietary driver unit (TSD Single Axis; Baldor Electric Company, Fort Smith, AR, USA) as this also incorporates safety cut-outs that can be cleared in the same way. Recovery following an extended power outage occurs similarly; the radar restarts operation as soon as power becomes available.

2.2. Signal Acquisition and Preprocessing

2.2.1. Fast Data Acquisition

The IMRs acquired radar echo signals via a bank of analogue-technology gated sample-and-hold circuits (Figure 2) that were built specifically for this purpose. The circuits produced steady output voltages that could be digitized to reasonable precision (12 bits) at the low rates (kHz) that were achievable with the analogue-to-digital (A-to-D) conversion technology available in the 1990s. Each gate was paired with a low-pass filter that effectively produced a running average over a sequence of pulses, improving the signal-to-noise ratio (SNR) and eliminating any higher frequencies—but this process also introduced a delay. Digitization occurred at the filter outputs at 320 Hz, i.e., after every fourth pulse [17]. This system of data acquisition in 'slow time' (in the parlance of radar signal processing) produced a lot of useful data (e.g., [9,10]), but the fixed broad gates introduced some contamination (see below). The availability from the mid-2000s of affordable and fast A-to-D converters provided an opportunity to both eliminate a demanding in-house hardware build and to improve the radar's data quality and coverage.

With fast data acquisition, the analogue circuitry is eliminated and the radar's 'video' output is directly converted into a sequence of digital values. For the non-coherent transceiver used in the IMRU, the video voltage is proportional to the logarithm of the intensity of the received signal. Echoes from targets at 2.55 km, the IMRU's maximum observing range, take 17 μs to return to the radar. Sampling along the 0–17-μs interval (i.e., in 'fast time') needs to be sufficiently frequent to discern the numerous echoes that the radar is capable of resolving over this range (Figure 2). Thus, A-to-D conversion at MHz frequencies is required. Echoes from a point target such as an insect have a nominal width of 0.05 μs when the IMRU is operating in S-mode, so a sampling frequency over 20 MHz ensures that echoes receive at least one digitization. However, while the transmitted pulse is approximately constant over its duration, the echo is rounded by the receiver's matching 20-MHz bandwidth (see, e.g., [12] (ch. 3)). The peak of the rounded echo provides accurate—and consistent—measures of both the signal intensity (the peak height) and the target's range (the time delay between transmission of the pulse and arrival of the echo). To obtain values for the peak, sampling at a rate significantly higher than 20 MHz ('oversampling') is needed. The IMRU uses a PCI 9820 converter (Adlink Technology, Taipei, Taiwan, China) which has maximum sampling rates of 120 MHz (single channel) or 60 MHz (two channels). The former, which was used in an earlier study [20], appears to be sufficient to locate the peak and determine its value by simply identifying the sample where the signal is strongest (Figure A1). The examples presented in this paper were acquired at 60 MHz, as the second channel was reallocated to a temporary system-integration test function (which does not need to be considered further here). At this

frequency, smoothing—as incorporated into the preprocessing, see below—or some other interpolative procedure may be needed to provide accurate peak determinations.

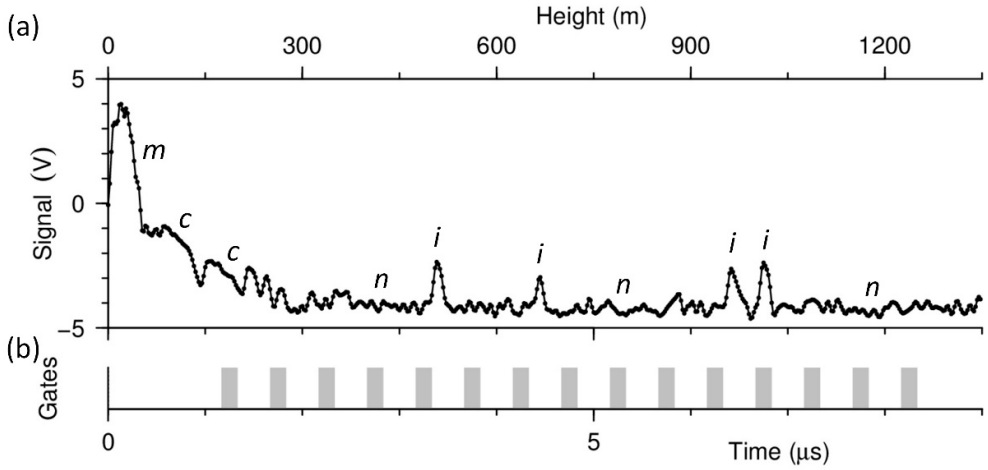

Figure 2. (**a**) Digitization at 60 MHz of an echo signal (a 'pulse pair'—see Appendix B) from the IMRU at Hay, NSW, on 1 December, 2018 at 21.31 h. Key: *m*—'main bang' (reverberation from transmitted pulse), *c*—ground clutter, *n*—receiver noise, and *i*—insect echo. (**b**) The gates used in the earlier Insect Monitoring Radars (IMRs).

Sampling is undertaken for each pulse, from 0–9 μs when the radar is operating in S-mode (Figure 2) and 8–17 μs when in M-mode. Each pulse produces 1080 samples, 540 for each channel; the sampling interval was then 0.167 μs, corresponding to 2.5 m in range. With a PRF of 960 Hz, this leads to 1,036,800 samples accumulating each second and ~187×10^6 over the 3-min duration of each data-acquisition session. The converter has 14-bit precision, so 2 bytes (8-bit) are needed to store each sample, for a total of ~373 Mbyte. During acquisition, the data accumulate on the PCI 9820 (which fits into a bus slot of a standard PC-type microcomputer); at the end of the 3-min session, they are transferred to the PC's main memory and immediately subjected to preprocessing. Only the outputs from preprocessing are stored to archival file: these vary in size but typically total ~300 Mbyte per day, to which ~200 Mbyte has to be added for the voucher files for a total of ~200 Gbyte per year. This quantity of data is practicable to retain on a terabyte storage device that can be exchanged and returned to the base laboratory during servicing visits. Full processing has not yet been implemented on a production basis, but it is envisaged that daily summaries will be produced for downloading via RDC, while the more detailed results that are needed for scientific analyses will be accumulated on the terabyte storage.

2.2.2. Video Amplifier

Both the video and the trigger outputs from the transceiver are mismatched for the inputs of the PCI 9820, and an interface unit had to therefore be built. Both voltage ranges and impedances (75 and 50 Ω) need changing. The video enters as a negative-going signal of amplitude ~1 V. To match this well to the −5 to +5 V input range of the A-to-D, the signal is inverted, amplified, and offset so that it extends over the range −4 to +4 V (Figure 2). This allows for the full exploitation of the 14-bit precision of the PCI 9820. In practice, echo signals from insects never approach saturation (at around +4 V), so the dynamic range of the signal data from insect targets is typically about 12 bits (precision ~0.02%). The video circuitry maintains the 20-MHz bandwidth of the receiver and required careful design to avoid signal distortion and spontaneous oscillation.

2.2.3. Elimination of Fixed Gates

It would have been straightforward to have reproduced the functioning of the IMR's analogue gates (although not that of the accompanying low-pass filters) in software, using the 60-MHz (or 120-MHz) digitizations as input. However, gating—at least when implemented as fixed broad gates—has significant drawbacks (see Appendix A). A more sophisticated form of preprocessing was therefore developed in which echoes are first recognized and located, and then a narrow (and, if necessary, moving) gate is formed over the echo (in software) and used to extract the signal pulse by pulse (see below). The resulting sequences substitute well for the outputs of the IMR's analogue gate circuits, though they differ from them in three respects: higher frequencies are not filtered out, there is no delay, and they are much less prone to the errors and distortions described in Appendix A. A great advantage of this approach is that echoes could be recognized and reconstructed throughout the entire 9-μs long sampling range, as the significant gaps that have to be left between fixed broad gates (see Appendix A) are eliminated. For the IMRU, this provides a 3-fold increase (over its IMR predecessors) in the number of echoes available for analysis in each 3-min sample. On an hourly basis, the increase is almost 5-fold, as there are more S-mode observing periods, and they last a little longer than the IMR ones. A more detailed description of the preprocessing algorithm that implements the moving gate is provided in Appendix B.

The sample numbers of the peak position provide a precise measure of the time interval Δt taken for the pulse to reach the target and return, and thus, by the usual radar relationship $R = c\Delta t/2$, of the range R. As the beam is vertical, the range corresponds to height h. Though the 0.05-μs pulse length indicates a range resolution of 7.5 m, the pulse-to-pulse scatter on the R values that are estimated from the sample numbers is much less than this. The explanation for this is that after rounding, the echo peak is well defined and the rounding occurs consistently from one pulse to the next. An investigation made when the sampling rate was 120 MHz showed that, after averaging over the 64 sample numbers obtained in each cycle (see Appendix B), remarkably high values for range precision of ~0.13 and ~0.2 m were obtained for the S and M modes respectively [20]. As beam transits typically last a few seconds, this precision, over ten or more cycles, allows target ascent (or descent) rates to be estimated, in some cases with an uncertainty as low as 0.2 m s^{-2}. This has enabled phenomena not previously accessible with non-coherent radars to be observed [20]. With 60-MHz sampling, precision is reduced, but useful observations are still obtained.

2.2.4. Preprocessing Algorithm.

The aim of preprocessing is to extract the data that contain useful information from the recorded echo sequences and to save only these to an archival file for later full processing. Depending on the number of targets present, preprocessing allows for 98–100% of the data recorded by the A-to-D converter to be discarded. Preprocessing needs to be rapid so that the loss of observing time is minimized and accurate, not least because discarded data cannot be recovered.

The preprocessing algorithm developed for the IMRU has three principal functions: the identification of targets, the tracking of each target individually, and the use of the track to guide a narrow moving gate that extracts the target's varying intensity. 'Tracking' here means determining the range of the target and following it as it varies (due to the target ascending or descending) from pulse to pulse (i.e., in slow time). Tracks need to be maintained even if the echo falls below the noise level for a fraction of each scan cycle, though when this fraction is large, the track can be abandoned (or not initiated). Using a narrow gate that moves eliminates almost all the limitations of fixed broad gates identified in Appendix A. When target densities are high, however, the extraction of individual echoes becomes impossible as targets overlap and interfere, so these echoes cannot be separated. To maintain some information output in these circumstances, the algorithm also calculates and saves average signal levels over a contiguous series of intervals spanning the full observation range. These averages can be drawn on to provide a general indication of insect activity and its variation with height, as well as to

avoid incorrectly inferring that insect numbers are low when a paucity of extracted echoes has in fact arisen through crowding.

The algorithm progresses in 10 stages, the details of which are provided in Appendix B and the Supplementary Materials. A preliminary data-compression stage reduces the 128 pulses from each antenna rotation cycle to 64 'pulse pairs'. Targets are then identified though a rather involved procedure that incorporates smoothing, peak-detection, and counting peak detections in each cycle (stages 2-8). The output from stage 8 is a series of 'linkages,' each of which associates the echo from a particular target from one cycle to the next. A linkage's running-average position forms the track that guides the narrow moving gate used to recover the echo signal (stage 9). As with the broad gates discussed previously, the highest value within the gate's window is selected. However, because the gate encompasses only the top of the rounded echo peak, there is no chance of its output transferring to a stronger nearby echo or of recording a point on the echo's shoulder rather than its peak, as happens when a gate is fixed and broad (Appendix A). The procedure sometimes outputs concatenations of two or more echoes, and these are split in a final stage 10.

3. Results

Four examples of IMRU observations of phenomena involving insects ascending and descending during migratory flight have been presented previously [20]. We present here, as a more general example of the IMRU's capabilities, observations of a nocturnal migration in which a distinct layer concentration developed and later dissolved (Figure 3). Such layers can form through a range of behavioural responses to a variety of environmental cues [12] (ch. 10). Determining the specific interactions of behaviour and atmospheric phenomena that have led to the formation of a layer remains challenging, especially for examples, such as this one, that form well above the surface, beyond the likely extent (at this stage of the night) of the surface temperature inversion.

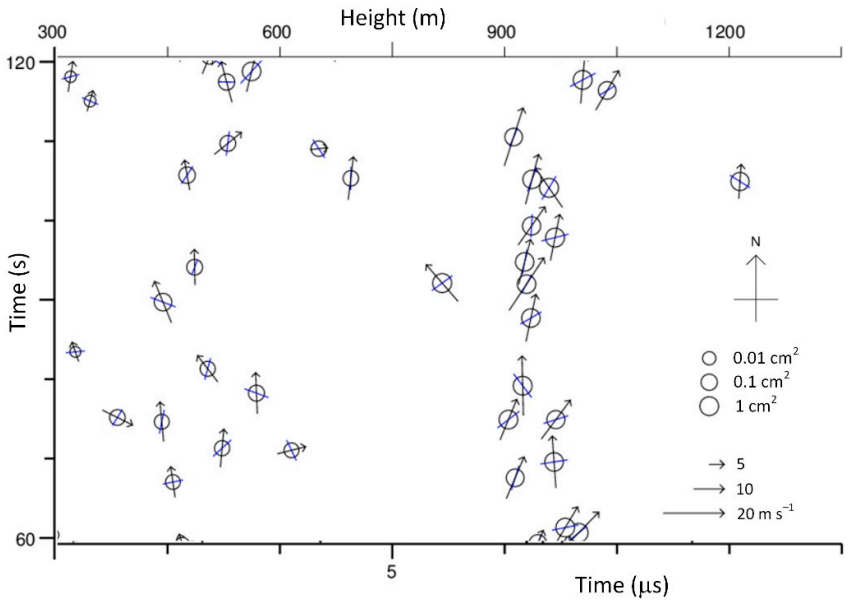

Figure 3. Graphical representation of output from full processing of 1 min of IMRU S-mode (pulse duration 0.05 μs) observations at Hay, NSW, on 29 November, 2019 at 22.09 h AEST (UTC+10). The short lines through each open circle indicate the target's alignment. Only targets for which all parameters could be retrieved are presented. Observations below 300 m were severely affected by ground clutter and have been omitted.

An inspection of Figure 3 indicates that the layer was located at around 950 m above the surface and was approximately 100 m deep. It comprised large insects, with polarization-averaged ventral-aspect radar cross-sections (RCSs) a_0 of about 1 cm^2, corresponding to masses of 100–300 mg [12] (ch. 4).

Known migrant species in this mass range that are found in inland New South Wales (NSW) include a number of larger noctuid moths and smaller specimens of *C. terminifera*. The layer targets were moving towards the NNE at speeds of 15–20 m s^{-1}. Alignments were more varied, but a NE/SW trend is evident. (ZLC radar observations determine the alignment of an insect's body axis, i.e., an angle in the range 0–180°, but do not resolve whether the insect is heading towards or away from this direction. Simultaneous measurements, or estimates, of the wind at the height of each target are needed to overcome this limitation [10], which also exists for alternative, e.g., scanning, radar configurations [12] (ch. 7).) Both above the layer and immediately below it, there were few insects, but below ~750 m, insects were again present. However, many of these were smaller (RCSs 0.01–0.1 cm^2, masses 30–100 mg), moving more slowly (10–15 m s^{-1}) and towards the N or NNW, and had more varied alignments.

A height–time plot of the fully analysed echoes from all the 3-min observation periods between 20.00 and 02.00 h (Figure 4) indicates that the layer formed around 21.15 h when a thinning of targets at ~900 m started to become evident. At 22.00 h, the layer started to rise, reaching ~1300 m at midnight (by which time M-mode observations were needed to follow it) and becoming more clearly separated from the migration below. A histogram of target sizes a_0 (Figure 5) suggests three populations that were separated by troughs at −6 and −20 dBsc. By partitioning the targets at these points, it becomes evident that the layer comprised only the 'large' types (a_0 peaking at 0 dBsc). These were also present below the layer, which had dissipated by 01.00 h (after which the large targets were spread fairly evenly throughout the height range 500–2000 m). 'Medium-sized' targets (a_0 peaking at −13 dBsc) were mainly confined to the region below 800 m once the layer had formed. This simple interpretation must be treated with caution, as larger targets are detectable to greater heights than smaller ones, and the observation ceiling for the medium targets is around 1 km [15]. Nevertheless, medium targets were observed to 1100 m at 21.00 h but were almost absent from the layer between 21.15 and 22.30 h when it was at or below this height. Thus, it appears that the medium-sized insects did not accompany the large ones into the layer.

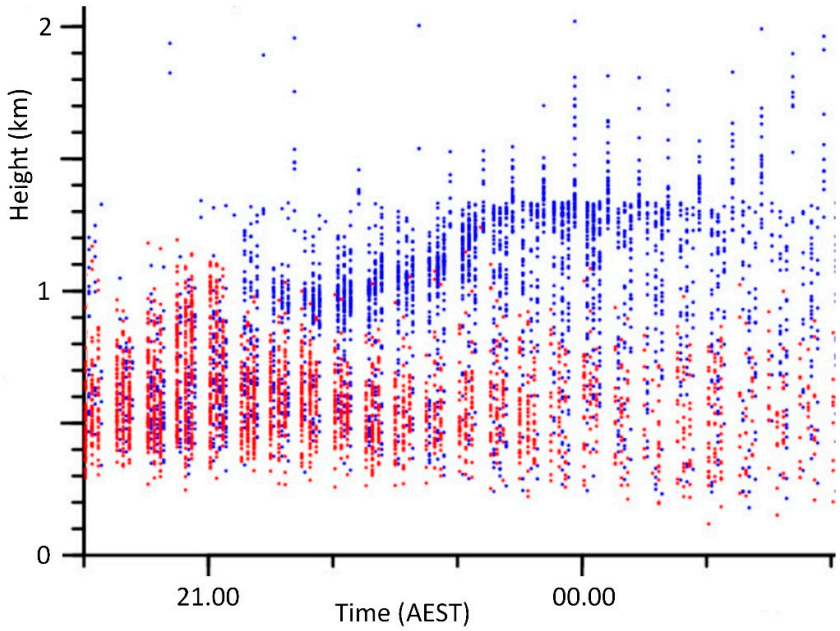

Figure 4. Height–time plot for IMRU observations at Hay, NSW, during part of the night of 29–30 November, 2019. Dusk (end of civil twilight) was at 19.45 h. Targets with a radar cross-section (RCS) a_0 > −6 dBsc (0.25 cm^2) shown in blue. Small targets (a_0 < −20 dBsc) have been omitted for clarity; they were detectable only to about 500 m.

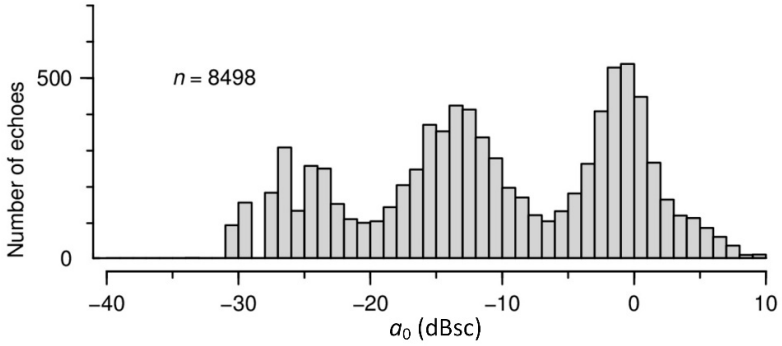

Figure 5. Histogram of RCS a_0 values for the target sample of Figure 4.

The shapes of the large targets fell into the 'main cluster region' (MCR; see [8]) of the shape-parameter (α_2, α_4) plane, while those of the medium targets fell into both the MCR and an extension of it to lower α_2 values (down to α_2 = 0.3) (Figure 6). The large targets met the criteria for the 'type-D' class recognized by Hao et al. [9]. Medium targets usually have shapes in the MCR, so many of those recorded here were typical examples of targets of that size; those with lower α_2 values perhaps had less elongated bodies than is usual in nocturnal migrants. Type-D and typical medium targets, if flying at night, can be tentatively identified as moths [9]. Wingbeat frequencies (not shown) were predominantly in the range of 20–40 Hz, which is consistent with the moth identification. Wingbeats, which cannot always be retrieved, were available for 63% of the large targets but only 27% of the medium targets.

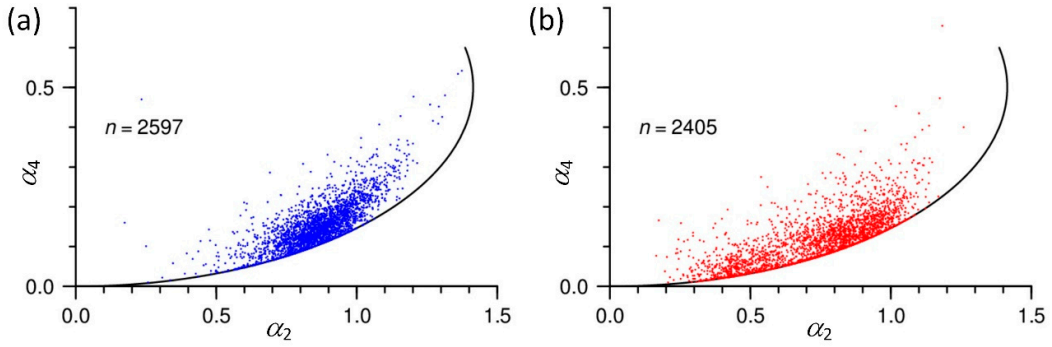

Figure 6. Scatter plots of shape parameters α_2 and α_4 for (**a**) the large and (**b**) the medium-sized targets in Figure 4. The curve indicates the boundary of the possible values of α_2 and α_4.

An inspection of graphical outputs like those in Figure 3 showed that the direction of the migration changed little during the first few hours, but the higher-flying insects were heading more to the NE after midnight and eventually, from about 03.00 h, to the E. During this later part of the night, the migration of medium-sized targets below 800 m became increasingly both thin and slow, though it was still directed to the N.

4. Discussion

The IMRU described here represents an attempt to extend the basic ZLC-configuration design, with its use of non-coherent pulse radar technology, to its limits. The aim was to maximize the amount of biologically useful data that this radar type can provide and to develop an observing facility of real utility for entomologists and aeroecologists. Two further considerations informed this approach. First, it was a relatively achievable objective given the resources available (principally the existing IMR units and expertise developed through operating them, maintaining them, and analysing their data); and second, biological analyses of IMR datasets had made evident that there were gaps in coverage that could usefully be filled, data samples that were quite frequently too small, and some indications of

data contamination. The rapid improvement in (affordable) data-acquisition and control technology since the 1990s, when the IMRs were designed, removed many of the limitations on data gathering and storage that had constrained the earlier design. Many of the improvements described here could be adapted for use in future entomological radars that employ more advanced radar technology, such as FMCW, pulse compression, polarimetry, or the use of millimetric wavelengths. Incorporating some of them may make the difference between a clever technological achievement and a long-term observing system that provides data that researchers can exploit.

The IMRU has operated satisfactorily at Hay over two insect-flight seasons. (Breaks in the observation series can mostly be attributed to faults developing in ageing subunits that were carried over from the IMRs.) Nevertheless, the specific parameters and thresholds mentioned here should be regarded as tentative: their optimal values have not yet been established. The present 15-min observing cycle, with 3 S and 1 M periods, each of 3 min, may also be modified. There may be a case for extending M observations downwards in order to increase the height range over which medium-sized targets can be observed. Similarly, it may be worthwhile to re-introduce stationary-beam observations, as the retrieval rate for wingbeat frequencies from rotating-polarization echoes is low for some target classes. The layer example presented here provides an instance in which both of these modifications might have been beneficial. However, any such extensions of the present protocol will decrease sample sizes and the continuity of the primary S- and M-mode datasets, and M-mode observations nearer the surface may be too affected by interference (due to the longer M pulses and the typically higher target densities lower down) to be useful. Another possible modification is a reduction of the antenna rotation rate to 270 r.p.m (4.5 Hz) and then averaging sets of four consecutive pulses rather than two. This would allow an increase in the PRF and provide a somewhat better SNR, but this would come at the cost of less frequent target-position fixes. As is usual in radar design and operation, priorities must be decided on, and compromises made accordingly. Modifications of these types require only changes to the operating software, and they could be remotely implemented via the communications link, perhaps only temporarily for a short-term trial.

The ability of IMRs and VLRs to operate autonomously, and the accumulation of extended observation datasets from locations far from the operators' base that this enables, greatly increases the utility of these units for both research and operational monitoring for pest management. If located within the coverage of a WSR, the detailed local information provided by the ZLC unit can be used to help interpret the observations of insect, bird, and bat movements over a much wider area that a high-power scanning radar can provide. A further possible application, foreshadowed nearly three decades ago [21], is the monitoring of general environmental health, as measured by insect numbers and their year-to-year variations. Here, the advantages of radar are that the monitoring process can be fully automated and that consistent and continuous measurements—in a relatively simple environment, the atmosphere, in which insects cannot hide—are provided. Specific identifications will not be achievable, and this will limit the technique's capacity to estimate biodiversity; however, as the example presented here demonstrates, partitioning of the radar counts, especially by size, is possible, so a series of information outputs could still be produced. The recent application of ZLC-radar observations to estimation of 'bioflows'—of pollinators, natural enemies, pollen, and nutrients [5]—illustrates the breadth of environmental-health issues that a radar-based monitoring network could address. Laser-based techniques also show promise in this role [22], but they have different capabilities and provide complementary rather than equivalent information; thus, the two technologies might be particularly effective if operated side-by-side.

5. Conclusions

Now over two decades old, the basic 'ZLC' radar design remains competitive as a means of observing and quantifying insect migration. It can determine all key migration parameters: the number of migrants, height, direction, speed, alignment, target size, and either two or three additional characters indicative of target identity. From these, the height profile of migration intensity and the

overall migration rate (and its direction) can be derived. With its ability to detect and characterize individual insects, as well as its consequent ability to partition the migrant population into different classes, it complements weather surveillance radars: while the latter scan over a wide area, they can provide information only about mixed ensembles of migrants. One weakness, the inability to resolve the 180° orientation ambiguity from radar data alone, is also shared by alternative observing systems.

The developments reported here show that the quality, continuity, and sample sizes of the data from a ZLC radar can be considerably improved over what is being produced by earlier implementations of this configuration. These improvements first arise through the adoption of modern digital technology for data acquisition, control, and storage; they secondly arise through the development of special software for operating the radar and extracting echo signals; and they thirdly arise through the use of the radar transceiver's 'medium pulse' operating mode to double the height range over which observations are made. As the examples here and in the previous paper [20] demonstrate, the upgraded radar is effective at revealing and examining the varied transient phenomena of insect migration, even when these extend to heights of over 2 km. The radar's capacity for accumulating long-term datasets at a modest cost suggests that it will similarly enable the development of insights into seasonal migration patterns and their inter-annual variations in response to ecological drivers. There also appears to be scope for a role in monitoring large-scale ecosystem health and its variation over decadal or even longer timescales.

Supplementary Materials: Software implementing the target-identification and signal extraction algorithm described in Section 2.2.4 and Appendix B is available online at http://www.mdpi.com/2072-4292/12/4/596/s1.

Author Contributions: Conceptualization, project administration, funding acquisition, resources, analysis, writing—original draft preparation, V.A.D.; methodology/hardware, V.A.D., S.H., C.S.; software, V.A.D., S.H., H.W.; validation/system testing, V.A.D., C.S., H.W.; data curation, V.A.D., H.W.; writing—review and editing, all authors. All authors have read and agreed to the published version of the manuscript.

Funding: This research was funded initially by Australian Research Council Linkage Grant LP0348025 and completed with internal funding from UNSW Canberra and the Australian Plague Locust Commission.

Acknowledgments: IMRU development has been supported by UNSW Canberra technical and engineering staff. It built on earlier IMR subunit designs and implementations developed by former UNSW student I.T. Harman and workshop staff. The IMRU is accommodated on the Hay Field Station of UNSW Sydney.

Conflicts of Interest: The authors declare no conflict of interest. The funders had no role in the design of the study; in the collection, analyses, or interpretation of data; in the writing of the manuscript; or in the decision to publish the results.

Disclaimer: Mention of a commercial product does not constitute or imply endorsement. Products mentioned may no longer be available.

Appendix A

Problems Arising with Fixed Gates

A conventional sample-and-hold gate is opened after a fixed delay—from the transmission of the pulse in the case of a pulse radar—and closed after a second, usually shorter, delay. The maximum signal appearing at the gate input while the gate is open is held at the gate output for a long enough duration for the held value to be recorded. Gates therefore operate in fast time (see 2.2.1) to enable recording in slow time. The gate duration needs to be kept short so that the range (height in the case of a vertical-beam unit) of the target that produces the held signal is known with reasonable precision, and the probability of multiple signals being present in the gate is low. Therefore, to cover a useful proportion of the range over which observations need to be made, a bank of gates is typically required. The former IMRs used 15 gates with durations of 0.167 μs (which corresponds to a range interval of 25 m) that were separated by gaps 0.333 μs (50 m) long (Figure 1). These design choices were informed by a need for good range resolution, an awareness of some of the problems discussed in this Appendix, and concerns about costs and system-complexity issues that would arise with an even larger number of gates.

Apart from the delay to opening, which determines the range at which the signal being sampled originates, the only gate parameter to be chosen is the 'width,' i.e., the duration for which the gate remains open. To accurately record a peak, the gate needs to encompass it (Figure A1a). Peak widths are determined by the duration of the transmitted pulse and the bandwidth of the receiver. For a strong peak, smoothing by the limited bandwidth will broaden the peak, at its base, to at least twice the pulse duration (Figure A1a). This suggests a criterion for a minimum gate width of 2–4× the pulse duration.

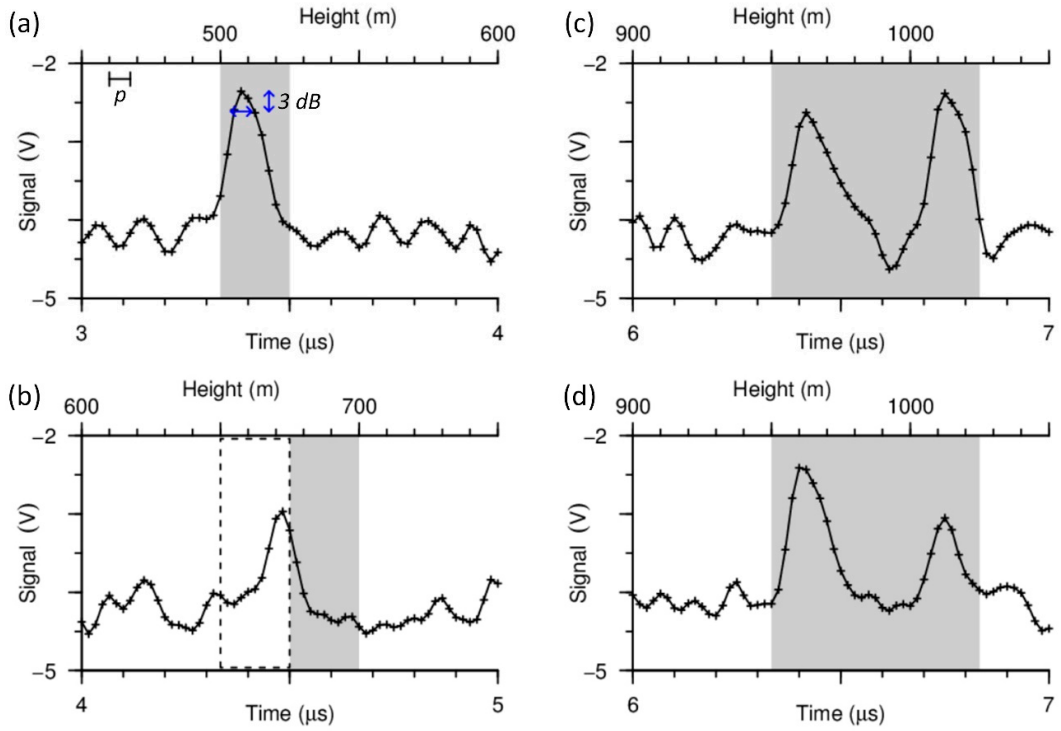

Figure A1. Actions of gates (grey) on echo signals. Signals are extracts from Figure 2. (**a**) Strong echo encompassed by gate of duration 0.167 μs (25 m). Key: *p*—width of transmitted pulse (0.05 μs, 7.5 m); arrows—echo width 3-dB (0.26 V) down from peak and approximately equal to the pulse width. (**b**) Echo just below gate. Dashed rectangle indicates a supposed preceding and immediately adjacent gate. (**c**) Pair of echoes encompassed by a gate of duration 0.5 μs (75 m). (**d**) Same as (**c**), but for the pulse-pair recorded one-quarter of a cycle (33 ms) earlier, when the beam polarization differed by 90°.

With a fixed gate, it is not, of course, certain that the gate will encompass the peak (Figure A1b). The gate will still record the maximum signal, but it will arise from the echo's sloping rise or fall phase rather than from its peak, and it will be less than the true value. The chance of this happening is greater for narrow gates than for broader ones, but given the finite width of the stronger echoes, it cannot be made negligible without broadening the gates to such an extent that useful range resolution (100 m or less for IMRU observations) would be lost. There is evidence of this effect in analyses of IMR data: when echoes attributable to *C. terminifera* are numerous, a lower number of echoes with similar shape parameters [8] and wingbeat frequencies but smaller RCSs are often also present (see e.g., [9] (Figure 2b)). A further problem with these slope recordings is that if the target is changing its range, the recorded value will change rapidly as the sloping face of the echo moves relative to the gate boundary.

The recording of slope values introduces a second source of inaccuracy: if gates are too close, echoes will be double counted—once accurately and a second time with too low a value (Figure A1b). To avoid this, gates must be separated by at least the width of a strong echo. Thus, with gating, individual data-acquisition sessions should extend over only a proportion of the full observation range. Full coverage remains possible by stepping the gates out over a sequence of sessions [15,17], but the number of echoes acquired (i.e., the sample size) will still be reduced.

Some of these undesirable effects will arise less frequently if the gates are made broader, but an additional problem then arises: there may be two or more echoes within the gate (Figure A1c). If the echoes are steady, exhibiting just a slow rise and fall, as occurs when stationary-beam observations are made, the larger will be consistently recorded, the undesirable consequences will be limited to biases: echo numbers will be underestimated at higher densities, and larger targets will be represented disproportionately in the samples. (If the rises and falls are not synchronous, the gate output will at some point switch from one target to the other; this is not a great problem because echoes that are concatenated in this way are quite easily split—see Appendix B.) However, the intensity of ZLC echoes from insects rapidly varies because of the rotating polarization and small-angle scan, typically peaking twice during each cycle. Unless two insects have the same orientation, the phases of these variations will differ; the maximum signal in the gate will then flip rapidly between the two echoes (Figure A1c,d), producing a mixed reconstructed signal. An inspection of IMR echoes that failed analysis indicates that some probably formed in this way (A.D., unpublished data). (Note that this mechanism is distinct from the electromagnetic interference that occurs—and likewise renders the echo unanalysable—when two targets differ in range by less than a pulse length.)

Appendix B

Preprocessing Procedure

The preprocessing algorithm comprises 10 stages. Stage 1 performs a simple data compression. Digitization occurs for each pulse, of which there are 128 per antenna-rotation cycle. Angular resolution as high as this seems unnecessary, so pairs of consecutive pulses are summed to produce 64 values per cycle. Summing is undertaken directly with the binary values, after clearing the two unused top bits. An additional factor of 2 is incorporated into the conversion of the binary values to voltages, so the effect is one of simple averaging. As receiver noise will be uncorrelated from one pulse to the next (i.e., across slow time), SNR will be improved (by a factor of $\sim \sqrt{2}$).

Target identification commences at stage 2, in which each pulse pair is smoothed by using a triangle function with a width close to that of the rounded echo: 5 samples wide for the S-mode (0.083 μs, or 13 m in range) and 17 (0.28 μs, 43 m) for the M-mode (Figure A2, which illustrates the process for an M-mode pulse-pair). These values are for 60 MHz sampling; for 120 MHz, the algorithm is identical, but these and other sample ranges are approximately doubled. The peaks in these smoothed sequences are identified in stage 3 by a simple procedure that identifies minima and maxima, ignoring fluctuations of 3 dB or less, and records peaks that rise 6 dB or more above the average level of the receiver noise (Figure A3). For S-mode echoes, these and all subsequent stages are applied only to ranges beyond the extent of the most severe ground clutter (90 m at Hay).

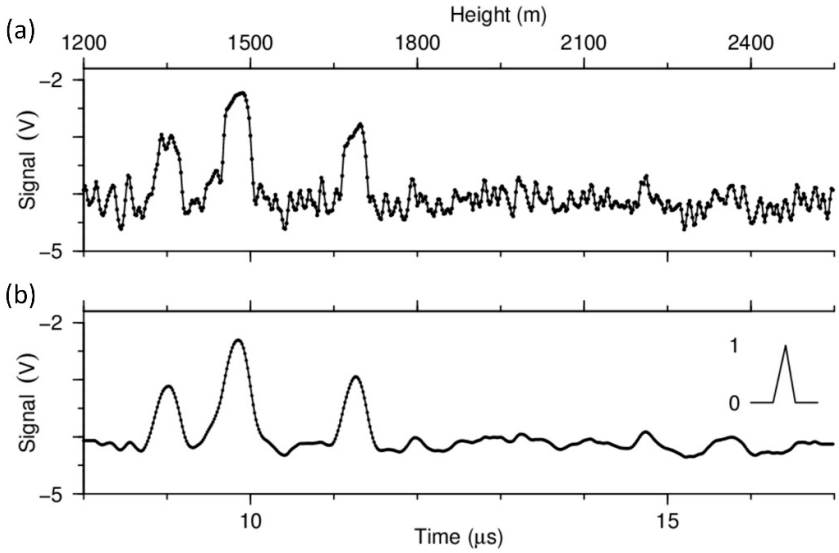

Figure A2. Pulse pair from the IMRU at Hay, NSW, on 1 December, 2018 at 21.41 h. (**a**) Digitized signal (slow-time average of two consecutive M-mode pulses). (**b**) Signal after fast-time smoothing with 17-sample wide triangle function (inset).

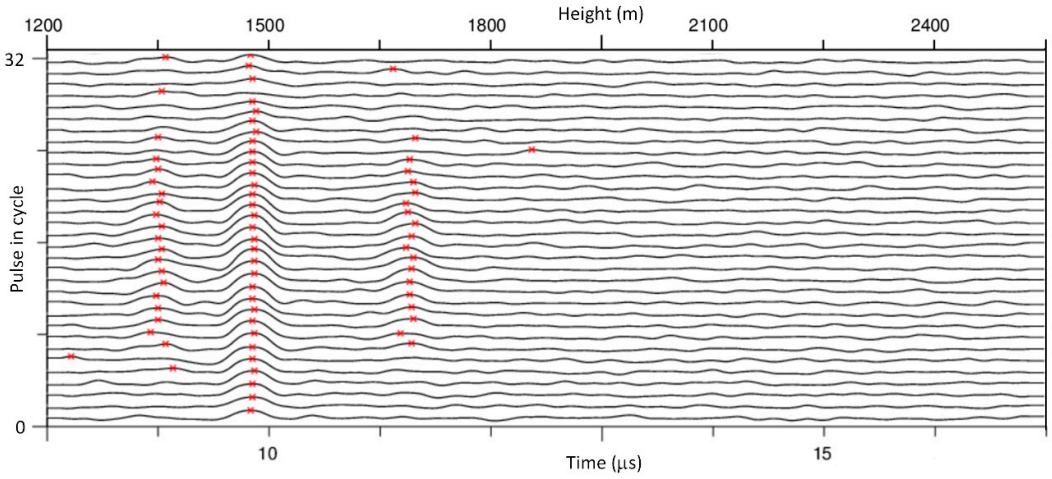

Figure A3. Waterfall plot showing the 32 smoothed pulse pairs from the first half of the cycle that included the pulse pair in Figure A2. Peaks identified in stage 3 are marked ×. The pulse pair shown in Figure A2 is at the mid-point of the sequence.

The next two stages consolidate all the pulse-pair peaks within a scan cycle. As the cycles last only 0.133 s, range changes due to target ascent or descent (typically at rates of <4 m s^{-1} [20]) will be less than the 2.5-m distance between samples. Therefore, the drift of the peaks within a cycle will be very slight. This consolidation allows the identity of an echo to be maintained even if the echo intensity falls below noise for some parts of the cycle (Figure A3). The approach used here is to count, for each 'section' of the observing range, the number of pulse-pairs in the cycle in which a peak is found (stage 4, Figure A4). A section consists of a single sample interval for S-observations and three adjacent sample intervals for M-observations (with their broader echoes), so there are 540 sections for S and 180 for M. In stage 5, these counts are smoothed both in range (fast time) and over cycles (i.e., in 'very slow time,' so termed as there are 64 slow-time intervals in each cycle). The initial smoothing is in range, with a triangle function with a width of 5 sections (stage 5a, Figure A4b). A peak is assigned to a single section of a pulse pair, with the adjacent sections empty. The function of this first smoothing is to integrate counts over adjacent sections in order to avoid the spuriously low values that arise when an echo straddles a section boundary. The triangle is therefore weighted to retain the 0-to-64

scale of the unsmoothed counts so that comparison with a detection threshold (at stage 6, see below) is straightforward. The second smoothing is over 5 successive cycles (stage 5b, Figure A5), and the triangle function is weighted conventionally (i.e., to conserve the total count) for this, as the stage 5a output values will vary only slowly from cycle to cycle if a persistent echo is present.

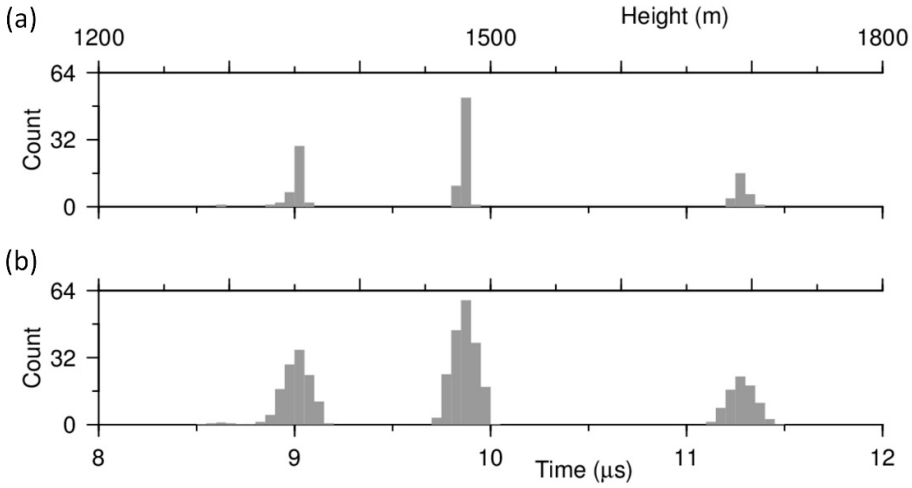

Figure A4. Histograms of counts of peaks identified in individual pulse pairs of the cycle shown in Figure A3 (terminated at 12 μs). (**a**) Counts. (**b**) Counts after smoothing with a triangle function extending over 5 histogram bins and weighted to maintain the peak count.

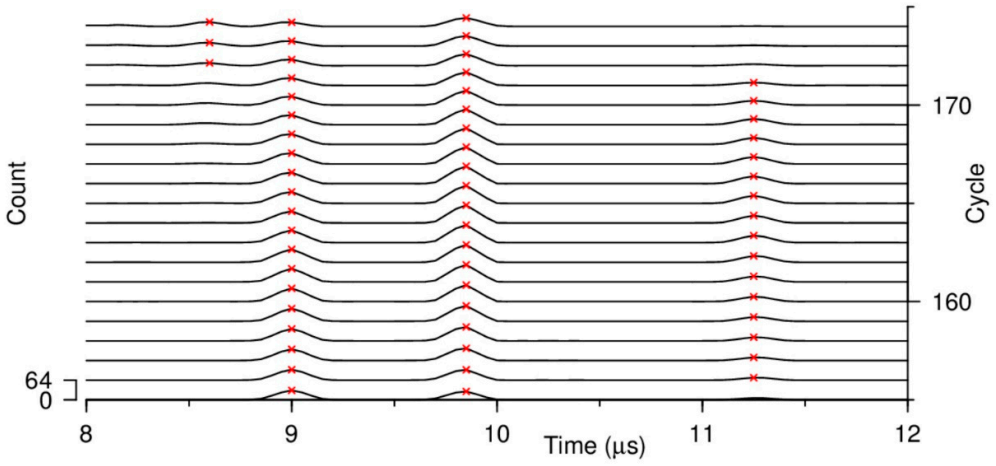

Figure A5. Waterfall plot showing a sequence of 20 doubly-smoothed cycle counts including, at number 164, the cycle of Figure A4. Peaks identified in stage 6 are marked ×.

In stage 6, peaks in fast-time are again identified, but this time by using the doubly smoothed counts to provide a single identification for each cycle (Figure A5). A threshold of only 8 counts, with fluctuations of up to 6 counts ignored, was adopted so that weaker echoes are detected and the durations (in very slow time) of stronger ones are maximized. These peaks are largely free of fluctuations and noise, and they thus provide a good basis for identifying and tracking targets. This occurs in stage 7, which links peaks in sequences of cycles. If a peak lies within a 5-section-wide window centred at the position (the section number) of an existing linkage, it is added to that linkage; if not, a new linkage is generated. Linkages are terminated as soon as no stage 6 peak is found within the linkage's search window. When a peak is added to a linkage, the linkage's position, calculated as a running average, is updated and recorded. A measure of link quality is also calculated and recorded; it indicates how close the new peak is, in both range and count, to the linkage's previous values for these quantities (Figure A6). When linking is completed (i.e., the final cycle of the 3-min dataset has

been processed), the accumulated linkages are reviewed, and very short ones (<4 cycles, the minimum length for which full analysis is possible) are culled (stage 8).

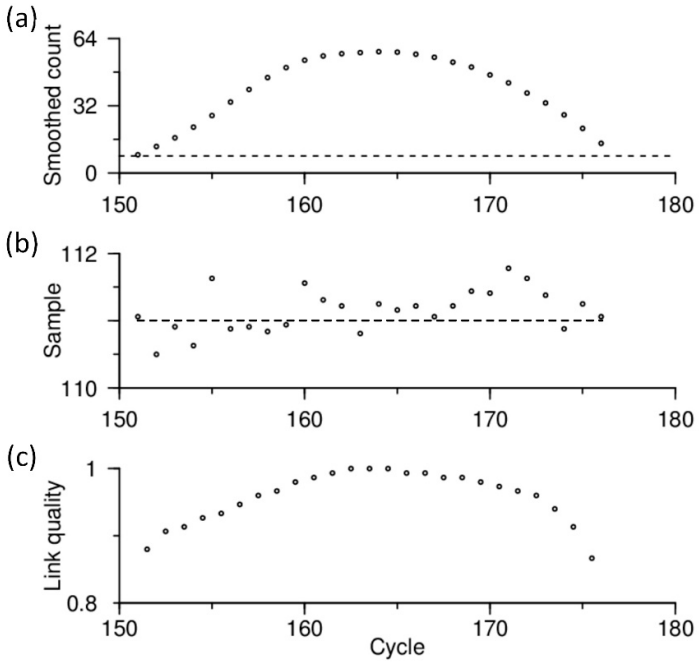

Figure A6. Linking of echo at 9.8 μs in Figure A5. (**a**) Smoothed count for each cycle; dashed line indicates threshold for inclusion in a linkage (8 out of the 64 pulse pairs). (**b**) Moving average linkage position (dashed line)) used to guide the narrow gate; in this example, it remained steady at sector 37. The points show the average position for each cycle of the smoothed peaks for each pulse pair, obtained by application of the narrow gate in stage 9. (**c**) Quality of links between successive cycles, on a scale of 0 (poor) to 1 (good).

The narrow moving gate that is used to extract the echo signal is centred on the linkage's running-average position (stage 9; Figure A6b). The gate is 7 samples wide for S-observations and 13 (samples, not sectors) for M-observations; these approximately correspond to the distances at which an echo from a point target will be 3 dB down from its peak value. The gate position is reset from the running average at the start of each cycle, and then this position is applied to each of the smoothed pulse-pairs (the stage 2 outputs, Figure A2b) in that cycle. The highest value within the gate's window is selected (Figure A7). The sequence of selections for the 64 pulse-pairs in each of the cycles included in the linkage forms the recovered echo signal for that target (Figure A8). This sequence is written to an output file along with the start time, the number of cycles, the position at each cycle (and its standard deviation), and the link quality value for each cycle.

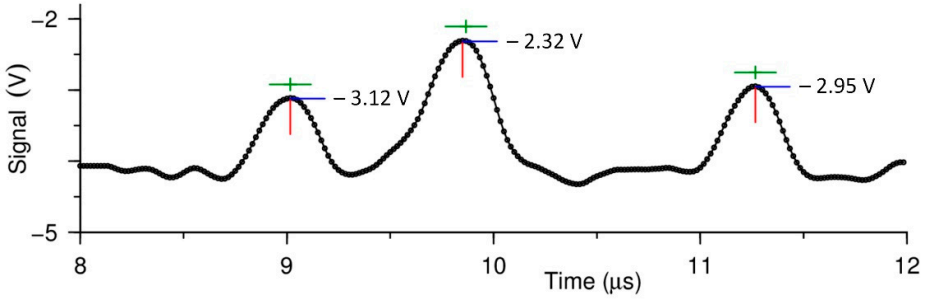

Figure A7. Smoothed pulse pair of Figure A2b (terminated at 12 μs) with the track centre and gate window (green) for the three identified echoes, as well as the retrieved peak positions (red) and intensities (blue).

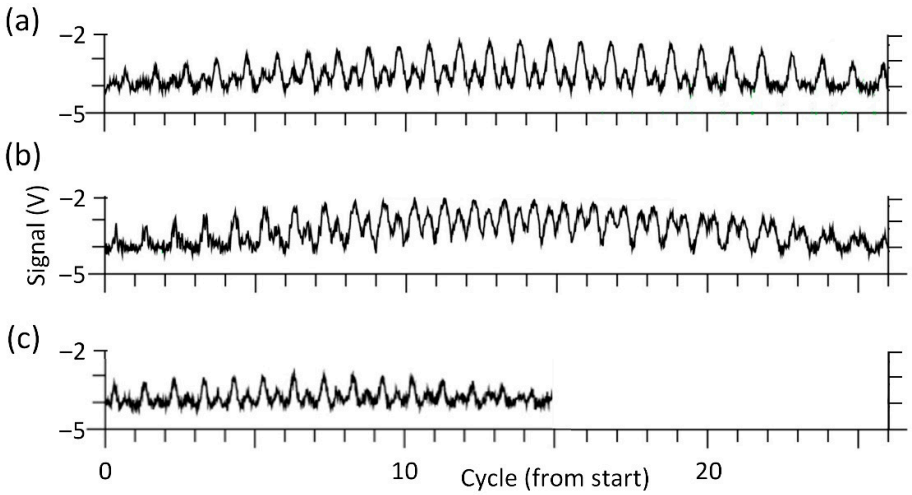

Figure A8. Echoes reconstructed with the narrow gate. Echoes are those at (**a**) 9.0 μs, (**b**) 9.8 μs and (**c**) 11.2 μs in Figure A2.

The recovered signals need to be subjected to one further procedure before they can be passed to the parameter-retrieval algorithm. It has been found that linking (stage 7) sometimes concatenates two or more nearby echoes, making a switch to a neighbouring peak when this becomes stronger than the one being followed. Such sequences usually exhibit more than one rise-and-fall, with a sudden change in target position and a decrease in link quality at the transition point. In stage 10, recovered signals are scanned for these features and split into individual echoes. For programming convenience, this procedure has been implemented as part of the full-processing algorithm, of which it forms the initial stage.

References

1. Beerwinkle, K.R.; Witz, J.A.; Schleider, P.G. An automated, vertical looking, X-band radar system for continuously monitoring aerial insect activity. *Trans. Am. Soc. Agric. Eng.* **1993**, *36*, 965–970. [CrossRef]
2. Drake, V.A. Insect-monitoring radar: A new source of information for migration research and operational pest forecasting. In *Pest Control and Sustainable Agriculture*; Corey, S.A., Dall, D.J., Milne, W.M., Eds.; CSIRO Publications: Melbourne, Australia, 1993; pp. 452–455.
3. Chapman, J.W.; Reynolds, D.R.; Smith, A.D. Vertical-Looking Radar: A new tool for monitoring high-altitude insect migration. *BioScience* **2003**, *53*, 503–511. [CrossRef]
4. Chapman, J.W.; Nesbit, R.L.; Burgin, L.E.; Reynolds, D.R.; Smith, A.D.; Middleton, D.R.; Hill, J.K. Flight orientation behaviors promote optimal migration trajectories in high-flying insects. *Science* **2010**, *327*, 682–685. [CrossRef] [PubMed]
5. Hu, G.; Lim, K.S.; Horvitz, N.; Clark, S.J.; Reynolds, D.R.; Sapir, N.; Chapman, J.W. Mass seasonal bioflows of high-flying seasonal migrants. *Science* **2016**, *354*, 1584–1587. [CrossRef] [PubMed]
6. Drake, V.A.; Wang, H. Recognition and characterization of migratory movements of Australian Plague Locusts, *Chortoicetes terminifera*, with an Insect Monitoring Radar. *J. Appl. Remote Sens.* **2013**, *7*, 075095. [CrossRef]
7. Westbrook, J.K.; Eyster, R.S. Doppler weather radar detects emigratory flights of noctuids during a major pest outbreak. *Remote Sens. Appl. Soc. Environ.* **2017**, *8*, 64–70. [CrossRef]
8. Drake, V.A. Distinguishing target classes in observations from vertically pointing entomological radars. *Int. J. Remote Sens.* **2016**, *37*, 3811–3835. [CrossRef]
9. Hao, Z.; Drake, V.A.; Taylor, J.R. Insect target classes discerned from entomological radar data. *Remote Sens.*. submitted.
10. Hao, Z.; Drake, V.A.; Taylor, J.R. Resolving the heading-direction ambiguity in vertical-beam radar observations of migrating insects. *Ecol. Evol.* **2019**, *9*, 6003–6013. [CrossRef] [PubMed]

11. Drake, V.A.; Gregg, P.C.; Harman, I.T.; Wang, H.K.; Deveson, E.D.; Hunter, D.M.; Rochester, W.A. Characterizing insect migration systems in inland Australia with novel and traditional methodologies. In *Insect Movement: Mechanisms and Consequences*; Woiwod, I., Reynolds, D.R., Eds.; CABI Publishing: Wallingford, UK, 2001; pp. 207–233. [CrossRef]
12. Drake, V.A.; Reynolds, D.R. *Radar Entomology: Observing Insect Flight and Migration*; CABI: Wallingford, UK, 2012.
13. Harman, I.T.; Drake, V.A. Insect Monitoring Radar: Analytical time-domain algorithm for retrieving trajectory and target parameters. *Comput. Electron. Agric.* **2004**, *43*, 23–41. [CrossRef]
14. Hu, C.; Li, W.; Wang, R.; Long, T.; Drake, V.A. Discrimination of parallel and perpendicular insects based on relative phase of scattering matrix eigenvalues. *IEEE Trans. Geosci. Remote Sens.* **2020**. [CrossRef]
15. Drake, V.A. Estimation of unbiased insect densities and density profiles with vertically pointing entomological radars. *Int. J. Remote Sens.* **2014**, *35*, 4630–4654. [CrossRef]
16. Reynolds, A.M.; Reynolds, D.R.; Smith, A.D.; Chapman, J.W. A single wind-mediated mechanism explains high-altitude 'non-goal oriented' headings and layering of nocturnally migrating insects. *Proc. R. Soc. B Biol. Sci.* **2010**, *277*, 765–772. [CrossRef] [PubMed]
17. Drake, V.A.; Harman, I.T.; Wang, H.K. Insect Monitoring Radar: Stationary-beam operating mode. *Comput. Electron. Agric.* **2002**, *35*, 111–137. [CrossRef]
18. Wang, H.K.; Drake, V.A. Insect Monitoring Radar: Retrieval of wingbeat information from conical-scan observation data. *Comput. Electron. Agric.* **2004**, *43*, 209–222. [CrossRef]
19. Drake, V.A.; Wang, H.K.; Harman, I.T. Insect Monitoring Radar: Remote and network operation. *Comput. Electron. Agric.* **2002**, *35*, 77–94. [CrossRef]
20. Drake, V.A.; Wang, H. Ascent and descent rates of high-flying insect migrants determined with a non-coherent vertical beam entomological radar. *Int. J. Remote Sens.* **2019**, *40*, 883–904. [CrossRef]
21. Riley, J.R. A radar technique for automatically monitoring insect migration and bio-diversity. In *Biotelemetry XII, Proceedings of the Twelfth International Symposium on Biotelemetry, Ancona, Italy, 31 August–5 September 1992*; Mancini, P., Fioretti, S., Cristalli, C., Bedini, R., Eds.; Editrice Universitaria Litografia Felici: Pisa, Italy, 1993; pp. 310–317.
22. Song, Z.; Zhang, B.; Feng, H.; Zhu, S.; Hu, L.; Brydegaard, M.; Li, Y.; Jansson, S.; Malmqvist, E.; Svanberg, K.; et al. Application of lidar remote sensing of insects in agricultural entomology on the Chinese scene. *J. Appl. Entomol.* **2019**. [CrossRef]